Journal of Physics: Condensed Matter

PAPER

Raman scattering investigation of the quasi-one-dimensional superconductor $Ta_4Pd_3Te_{16}$

To cite this article: D Chen *et al* 2015 *J. Phys.: Condens. Matter* **27** 495701

IOP Publishing Journal of Physics: Condensed Matter
J. Phys.: Condens. Matter **27** (2015) 495701 (6pp) doi:10.1088/0953-8984/27/49/495701

Raman scattering investigation of the quasi-one-dimensional superconductor $Ta_4Pd_3Te_{16}$

D Chen[1], P Richard[1,2], Z-D Song[1], W-L Zhang[1], S-F Wu[1], W H Jiao[3], Z Fang[1,2], G-H Cao[3] and H Ding[1,2]

[1] Beijing National Laboratory for Condensed Matter Physics, and Institute of Physics, Chinese Academy of Sciences, Beijing 100190, People's Republic of China
[2] Collaborative Innovation Center of Quantum Matter, Beijing, People's Republic of China
[3] Department of Physics, Zhejiang University, Hangzhou 310027, People's Republic of China

E-mail: p.richard@iphy.ac.cn

Received 2 September 2015, revised 15 October 2015
Accepted for publication 28 October 2015
Published 23 November 2015

Abstract

We have performed polarized Raman scattering measurements on the newly discovered superconductor $Ta_4Pd_3Te_{16}$ ($T_c = 4.6$ K). We observe 28 out of 33 Raman active modes, with frequencies in good accordance with first-principles calculations. Although most of the phonons observed vary only slightly with temperature and do not exhibit any asymmetric profile that would suggest strong electron–phonon coupling, the linewidth of the A_g phonon mode at 89.9 cm^{-1} shows an unconventional increase with temperature decreasing, which is possibly due to a charge-density-wave transition or the emergence of charge-density-wave fluctuations below a temperature estimated to fall in the 140–200 K range.

Keywords: $Ta_4Pd_3Te_{16}$, 1D superconductor, Raman, phonons

(Some figures may appear in colour only in the online journal)

1. Introduction

Because they have anisotropic interactions and electronic properties, low-dimensional systems often show intriguing physical behaviours. Despite a low critical temperature (T_c) of 4.6 K [1], the newly discovered quasi-one-dimensional (quasi-1D) superconductor $Ta_4Pd_3Te_{16}$ has been labelled as an unconventional superconductor from scanning tunnelling microscopy (STM) [2] and thermal conductivity [3] experiments, from which an anisotropic gap structure with possible nodes has been proposed. This result is quite intriguing since the electronic states of typical unconventional superconductors at the Fermi level are derived from *d* or *f* bands while a recent density functional theory (DFT) study on $Ta_4Pd_3Te_{16}$ indicates that they mainly originate from Te *p* states in this material with only little contribution from *d* electrons from transition metal elements [4]. In addition, quasi-1D systems are particularly prone to the formation of a static charge-density-wave (CDW) or a static spin-density-wave (SDW), often regarded as states in competition with superconductivity. Not only does the electronic structure contain nested Te *p* bands, which would be favourable to a CDW rather than a SDW [4], a CDW-like gap feature has also been reported from low-temperature STM measurements on stripes of Te atoms [5]. CDW fluctuations are thus a potential candidate for the pairing glue in $Ta_4Pd_3Te_{16}$ that would in principle favour a singlet state [4] and strong electron–phonon interactions.

In order to investigate the strength of the electron–phonon coupling and the possible existence of a CDW instability, here we present a Raman scattering study of $Ta_4Pd_3Te_{16}$ supported by first-principles calculations of the vibration modes. Raman scattering is an experimental technique very sensitive to modulations in the lattice that is also capable of probing electron–phonon interactions. We observed 28 out of 33 Raman active modes, with frequencies in good accordance with our first-principles calculations. Most of the phonons that we observed suggest no strong electron–phonon coupling and vary only slightly

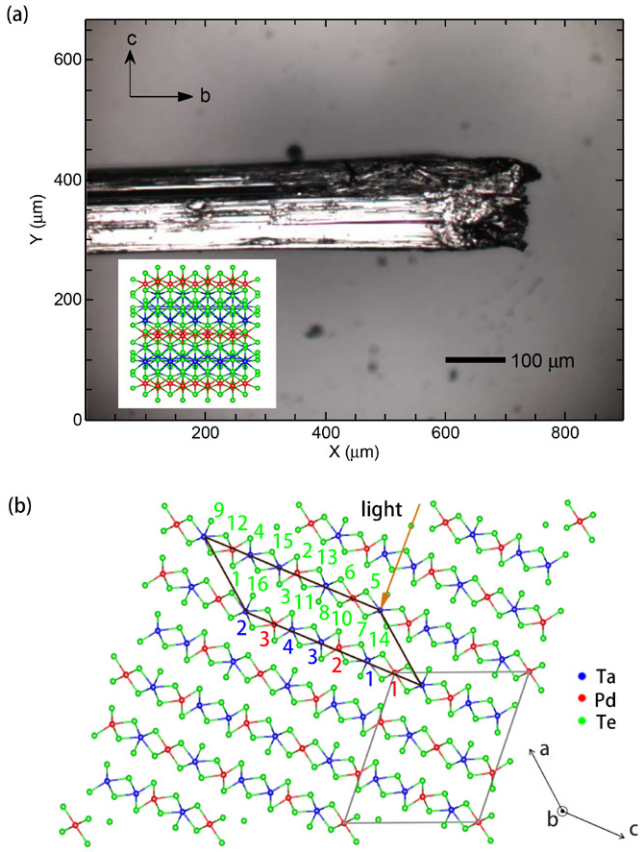

Figure 1. (a) Photo of a $Ta_4Pd_3Te_{16}$ single crystal. The inset shows the crystal structure viewed perpendicularly to the sample surface. (b) Crystal structure of $Ta_4Pd_3Te_{16}$ viewed perpendicularly to the *b*-axis. The black parallelogram represents the primitive cell used in our Raman measurements, while the grey one refers to another unit cell commonly used. All the atoms in the primitive cell are identified by numbers. The incident light is perpendicular to the *bc* plane.

with temperature, except for one A_g phonon at 89.9 cm^{-1}. We show that this particular mode, associated to vibrations of Te located along the stripes where a CDW-like gap was observed from STM [5], splits in the 140–200 K temperature range and below, which is possibly related to a CDW transition or CDW fluctuations.

2. Experiment

The $Ta_4Pd_3Te_{16}$ single crystals used in our Raman scattering measurements were prepared by a self-flux method [1]. The shiny, soft, layered samples have a typical dimension of $2.5 \times 0.1 \times 0.05$ mm^3, as shown in figure 1(a). Raman scattering measurements were performed using 488.0 nm, 514.5 nm, 530.9 nm, 568.2 nm and 676.5 nm laser excitations in a back-scattering micro-Raman configuration with a triple-grating spectrometer (Horiba Jobin Yvon T64000) equipped with a nitrogen-cooled CCD camera. At room temperature a 100× objective was used to both focus the laser beam and collect the scattered light whereas a long-focus distance 50× objective was used for measurements in the low-temperature cryostat. The crystals were cleaved by tape to obtain clean and flat surfaces, and then transferred into a

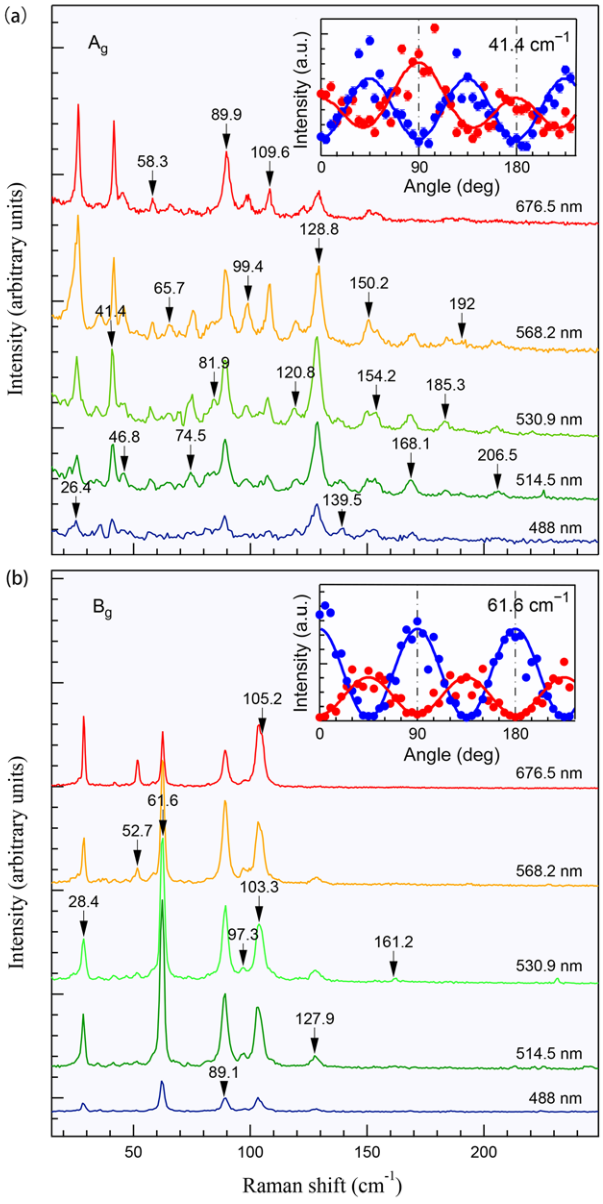

Figure 2. (a) A_g modes recorded with 488.0 nm, 514.5 nm, 530.9 nm, 568.2 nm and 676.5 nm laser excitations under the (*YY*) polarization configuration at room temperature. The curves are shifted relative to each other for clarity. The inset shows the intensity of the peak at 41.4 cm^{-1} as a function of the in-plane angle with respect to the *b* axis. The red dots and blue dots are measured under parallel and perpendicular polarization configuration, respectively. The blue and red lines are fits of the experimental data based on the A_g tensor. (b) Same as (a) but for the B_g modes recorded under the (*YZ*) polarization configuration at room temperature.

low-temperature ST500 (Janis) cryostat for the Raman measurements between 5 and 350 K with a working vacuum better than 2×10^{-6} mbar. In this paper we use the primitive cell represented by the black line in figure 1(b), which differs from the unit cell used in previous reports [6, 7] on this material (grey line). We define *Y* and *Z* as the directions along the *b* and *c* axes, respectively. The *Y* direction corresponds to the $PdTe_2$ chains direction. The natural cleaved surface of this crystal is the Ta–Pa–Te layer, i.e. the *bc* plane, as evidenced by STM measurements [2].

Table 1. Comparison of the calculated and experimental Raman active phonon modes at 294 K.

Sym.	Exp.	Cal.	Main atom displacements
A_g	26.4	21.0	$Pd^2(-xz)$, $Pd^3(xz)$, $Te^9(xz)$, $Te^{10}(-xz)$, $Te^{15}(-xz)$, $Te^{16}(xz)$
B_g	28.4	27.9	$Ta^1(y)$, $Ta^2(-y)$, $Pd^2(y)$, $Pd^3(-y)$, $Te^8(y)$, $Te^9(-y)$, $Te^{15}(y)$, $Te^{16}(-y)$
A_g	41.4	36.9	$Ta^1(xz)$, $Ta^2(-xz)$, $Te^1(-xz)$, $Te^2(xz)$, $Te^5(xz)$, $Te^6(-xz)$, $Te^{15}(xz)$, $Te^{16}(-xz)$
A_g	46.8	41.6	$Ta^1(-z)$, $Ta^2(z)$, $Pd^2(xz)$, $Pd^3(-xz)$, $Te^3(xz)$, $Te^4(-xz)$, $Te^{13}(-z)$, $Te^{14}(z)$
B_g	52.7	48.2	$Ta^1(-y)$, $Ta^2(y)$, $Pd^2(y)$, $Pd^3(-y)$, $Te^5(-y)$, $Te^6(y)$, $Te^7(-y)$, $Te^8(y)$, $Te^9(-y)$, $Te^{10}(y)$
A_g	58.3	58.3	$Ta^3(xz)$, $Ta^4(-xz)$, $Pd^2(-xz)$, $Pd^3(xz)$, $Te^3(z)$, $Te^4(-z)$, $Te^9(-xz)$, $Te^{10}(xz)$, $Te^{15}(-xz)$, $Te^{16}(xz)$
B_g	61.6	61.5	$Ta^3(-y)$, $Ta^4(y)$, $Pd^2(y)$, $Pd^3(-y)$, $Te^3(-y)$, $Te^4(y)$, $Te^{11}(-y)$, $Te^{12}(y)$, $Te^{15}(y)$, $Te^{16}(-y)$
A_g	65.7	62.1	$Pd^2(xz)$, $Pd^3(-xz)$, $Te^3(xz)$, $Te^4(-xz)$, $Te^7(-xz)$, $Te^8(xz)$, $Te^{15}(-z)$, $Te^{16}(z)$
A_g	74.5	74.8	$Ta^3(-xz)$, $Ta^4(xz)$, $Te^1(-xz)$, $Te^2(xz)$, $Te^3(-xz)$, $Te^4(xz)$, $Te^9(xz)$, $Te^{10}(-xz)$
A_g	81.9	81.9	$Ta^3(-xz)$, $Ta^4(xz)$, $Te^5(-z)$, $Te^6(z)$, $Te^{11}(xz)$, $Te^{12}(-xz)$, $Te^9(xz)$, $Te^{10}(-xz)$
B_g	89.1	87.2	$Te^9(-y)$, $Te^{10}(y)$, $Te^{15}(-y)$, $Te^{16}(y)$
A_g	89.9	87.8	$Te^1(-xz)$, $Te^2(xz)$, $Te^5(-xz)$, $Te^6(xz)$, $Te^7(xz)$, $Te^8(-xz)$
B_g	97.3	96.5	$Te^5(y)$, $Te^6(-y)$, $Te^7(-y)$, $Te^8(y)$, $Te^{13}(y)$, $Te^{14}(-y)$
A_g	99.4	99.8	$Te^1(xz)$, $Te^2(-xz)$, $Te^3(-xz)$, $Te^4(xz)$, $Te^5(z)$, $Te^6(-z)$, $Te^7(xz)$, $Te^8(-xz)$, $Te^{13}(xz)$, $Te^{14}(-xz)$
B_g	—	100.6	$Te^3(y)$, $Te^4(-y)$, $Te^{11}(-y)$, $Te^{12}(y)$
B_g	103.3	101.4	$Te^1(y)$, $Te^2(-y)$, $Te^5(y)$, $Te^6(-y)$
B_g	105.2	105.1	$Te^1(-y)$, $Te^2(y)$, $Te^7(-y)$, $Te^8(y)$, $Te^{13}(-y)$, $Te^{14}(y)$
A_g	109.6	109.4	$Te^3(xz)$, $Te^4(-xz)$, $Te^5(-xz)$, $Te^6(xz)$, $Te^{13}(-xz)$, $Te^{14}(xz)$
A_g	—	116.2	$Te^7(-xz)$, $Te^8(xz)$, $Te^9(-xz)$, $Te^{10}(xz)$, $Te^{15}(xz)$, $Te^{16}(-xz)$
A_g	120.8	120.2	$Te^5(xz)$, $Te^6(-xz)$, $Te^7(-z)$, $Te^8(z)$, $Te^{15}(-xz)$, $Te^{16}(xz)$
A_g	—	125.2	$Pd^2(xz)$, $Pd^3(-xz)$, $Te^3(-xz)$, $Te^4(xz)$, $Te^{11}(xz)$, $Te^{12}(-xz)$
A_g	128.8	125.4	$Te^5(-xz)$, $Te^6(xz)$, $Te^{13}(xz)$, $Te^{14}(-xz)$
B_g	127.9	128.5	$Ta^3(y)$, $Ta^4(-y)$, $Te^3(-y)$, $Te^4(y)$
A_g	139.5	138.0	$Pd^2(-xz)$, $Pd^3(xz)$, $Te^9(-xz)$, $Te^{10}(xz)$, $Te^{11}(xz)$, $Te^{12}(-xz)$, $Te^{15}(-z)$, $Te^{16}(z)$
A_g	150.2	148.7	$Pd^2(xz)$, $Pd^3(-xz)$, $Te^3(-xz)$, $Te^4(xz)$, $Te^{11}(z)$, $Te^{12}(-z)$
A_g	154.2	149.6	$Te^1(-xz)$, $Te^2(xz)$, $Te^5(-xz)$, $Te^6(xz)$, $Te^7(-z)$, $Te^8(z)$,
B_g	—	157.3	$Pd^2(-y)$, $Pd^3(y)$, $Te^9(-y)$, $Te^{10}(y)$, $Ta^{15}(y)$, $Ta^{16}(-y)$
B_g	161.2	161.2	$Ta^1(y)$, $Ta^2(-y)$, $Te^5(-y)$, $Te^6(y)$, $Te^7(-y)$, $Te^8(y)$,
A_g	168.1	167.3	$Pd^2(xz)$, $Pd^3(-xz)$, $Te^{15}(-z)$, $Te^{16}(z)$
A_g	—	180.6	$Ta^3(-xz)$, $Pd^4(xz)$, $Te^3(-xz)$, $Te^4(xz)$, $Te^9(-xz)$, $Te^{10}(xz)$
A_g	185.3	187.3	$Ta^1(z)$, $Ta^2(-z)$, $Te^7(-z)$, $Te^8(z)$
A_g	192	193.0	$Ta^1(-xz)$, $Ta^2(xz)$, $Te^5(xz)$, $Te^6(-xz)$, $Te^{15}(xz)$, $Te^{16}(-xz)$
A_g	206.5	206.5	$Ta^3(xz)$, $Ta^4(-xz)$, $Pd^2(xz)$, $Pd^3(-xz)$, $Te^3(-xz)$, $Te^4(xz)$, $Te^9(xz)$, $Te^{10}(-xz)$

Note: The energies are given in cm^{-1}. The atoms are identified in figures 1(b).

3. Results and discussion

The $Ta_4Pd_3Te_{16}$ crystal structure is characterized by space group I2/m (point group C_{2h}). A simple group symmetry analysis [8] indicates that the phonon modes at the Brillouin zone (BZ) centre decompose into $[22A_g + 11B_g] + [11A_u + 22B_u] + [A_u + 2B_u]$, where the first, second and third terms represent the Raman-active modes, the infrared (IR)-active modes and the acoustic modes, respectively. To get estimates on the mode frequencies of $Ta_4Pd_3Te_{16}$, we employed the first-principles pseudopotential plane wave method package Quantum Espresso [9]. We set a $5 \times 5 \times 5$ Monkhorst-pack k point mesh and a 40 Ry cutoff for wavefunctions. Using the generalized gradiant approximation [10], we first relax both the cell and atom coordinates of experimental results [6] until the forces acting on atoms are all smaller than 10^{-4} Ry/a_B and the pressure is smaller than 0.2 kbar. Using the information on the ground state, it is easy to use the Phonon package which implements the density functional perturbation theory (DFPT) [11–13] to get the A_g and B_g phonon frequencies and vibration modes at the Γ point. The calculated phonon modes, their symmetries and the main atomic displacements involved, are given in table 1.

In figures 2(a) and (b), we show the Raman spectra of $Ta_4Pd_3Te_{16}$ recorded at room temperature under 488.0 nm, 514.5 nm, 530.9 nm, 568.2 nm and 676.5 nm laser excitations. In total, we observe no less than 28 of the 33 Raman active modes predicted. The scattered intensities of the five absent modes are too weak to be detected. As indicated in table 1, the

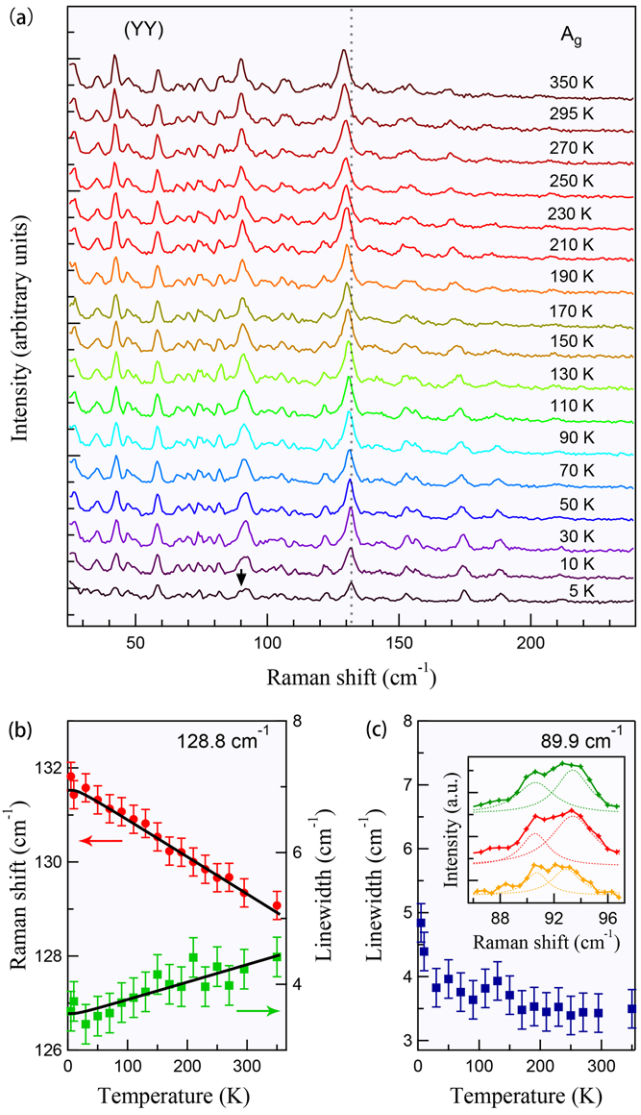

Figure 3. (a) Temperature dependence of the Raman spectra for the A_g modes. The curves are shifted relative to each other for clarity. The vertical dashed line and the arrow are guides to the eye. (b) Peak position (in red) and linewidth (full width at half maximum, in green), respectively, of the A_g mode at 128.8 cm^{-1}. The curves are fits to equations (2) and (3). (c) Peak linewidth of the A_g mode at 89.9 cm^{-1}. The inset shows the spectra of this peak at 5 K. The green spectrum is recorded with 514.5 nm laser excitation. The red and yellow spectra show this peak as measured from another sample with 514.5 nm and 568.2 nm laser excitations, respectively. The dashed lines are fits of the experimental data with two Lorentzian components.

experimental and calculated mode energies are in a very good agreement. Using the polarization selection rules and the fact that the *b* axis is easily determined by the morphology of the samples, the assignments of the Raman symmetries for each mode is straightforward. The Raman tensors corresponding to the C_{2h} symmetry group are expressed as:

$$A_g = \begin{pmatrix} a & 0 & d \\ 0 & b & 0 \\ d & 0 & c \end{pmatrix}, B_g = \begin{pmatrix} 0 & e & 0 \\ e & 0 & f \\ 0 & f & 0 \end{pmatrix}. \quad (1)$$

For perfectly aligned crystals, pure A_g symmetry is obtained in the (*YY*) configuration. In this channel, we detect 19 peaks at 26.4 cm^{-1}, 41.4 cm^{-1}, 46.8 cm^{-1}, 58.3 cm^{-1}, 65.7 cm^{-1}, 74.5 cm^{-1}, 81.9 cm^{-1}, 89.9 cm^{-1}, 99.4 cm^{-1}, 109.6 cm^{-1}, 120.8 cm^{-1}, 128.8 cm^{-1}, 139.5 cm^{-1}, 150.2 cm^{-1}, 154.2 cm^{-1}, 168.1 cm^{-1}, 185.3 cm^{-1}, 192 cm^{-1} and 206.5 cm^{-1}. They correspond to vibrations of atoms in the *bc* plane. Pure B_g symmetry is obtained in the (*YZ*) configuration. In this channel, we detect 9 peaks at 28.4 cm^{-1}, 52.7 cm^{-1}, 61.6 cm^{-1}, 89.1 cm^{-1}, 97.3 cm^{-1}, 103.3 cm^{-1}, 105.2 cm^{-1}, 127.9 cm^{-1}, and 161.2 cm^{-1}. They correspond to vibrations of atoms along the *b*-axis. The symmetric peak profiles that we observe suggest that the electron–phonon coupling is not particularly strong in this system.

We also checked how the peak intensities vary away from perfect orientation. Assuming, in a first approximation, that the matrix elements of the Raman tensors are real numbers, the intensity of the A_g modes should vary with the angle θ between the *b* axis and the incident polarization vector $\mathbf{e}_i$ as $|b\cos^2\theta + c\sin^2\theta|^2$ and $|(b-c)\sin 2\theta|^2$ for parallel and cross polarization configurations, respectively. For the cross polarization configuration, this implies a four-fold symmetry with maxima at 45 degrees and each successive 90 degrees, which is exactly what we observe for the A_g peak at 41.4 cm^{-1}, as shown in the inset of figure 2(a). For the parallel configuration, the expected angular dependence of the A_g peaks depends on the relative sign and intensity of the *b* and *c* elements in the Raman tensor. For the peak at 41.4 cm^{-1}, we observe small maxima at $\theta = 0$ and $\theta = 180$ degrees, a larger maxima at $\theta = 90$ degrees and four-fold minima starting at $\theta = 45$ degrees. This situation is only possible if *b* and *c* have a different sign and $|c/b| > 1$. Indeed, we found $c/b = -1.5$ from the fitting of the experimental data. The intensity of the B_g mode peaks should be proportional to $|f\sin 2\theta|^2$ and $|f\cos 2\theta|^2$ for parallel and cross polarization configurations, respectively. This coincides in both cases with four-fold oscillations, with the first maximum at $\theta = 45$ degrees and $\theta = 0$ degrees, respectively, in agreement with the results illustrated in the inset of figure 2(b) for the B_g peak at 61.6 cm^{-1}.

To investigate the possible role of the electron–phonon coupling and the possible existence of a CDW order, we cooled the samples down to 5 K. In figures 3(a) and 4(a), we display the temperature dependence of the A_g peaks and B_g peaks, respectively. As expected, most peaks are slightly blue shifted and become a little sharper with temperature decreasing, except for the A_g peak at 89.9 cm^{-1} that we discuss below. We show in figure 3(b), a quantitative analysis of the peak position and the linewidth of the A_g Raman peak at 128.8 cm^{-1}, which has been fitted with a Lorentzian function. The results of similar analysis are also shown in figures 4(b) and (c) for the B_g mode at 61.6 cm^{-1}. The peak position $\omega_{\rm ph}(T)$ and the linewidth $\Gamma_{\rm ph}(T)$ are consistent with simple expressions corresponding to the anharmonic phonon decay into acoustic phonons with the same frequencies and opposite momenta [14, 15]:

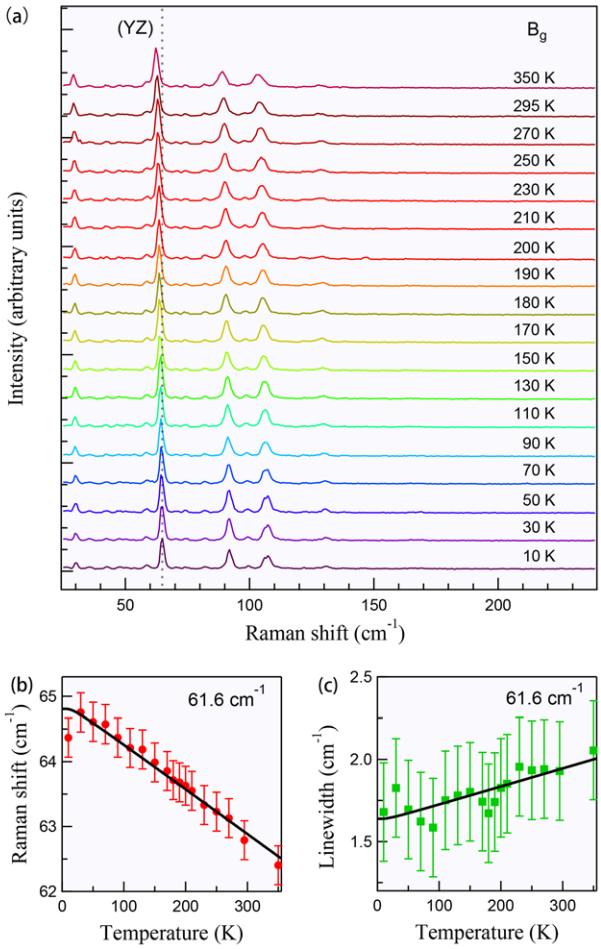

Figure 4. (a) Temperature dependence of the Raman spectra for the B_g modes. The curves are shifted relative to each other for clarity. The vertical dashed line is a guide to the eye. (b), (c) Peak position and linewidth (full width at half maximum), respectively, of the B_g mode at 61.6 cm^{-1}. The curves in (b), (c) are fits to equations (2) and (3).

$$\omega_{\rm ph}(T) = \omega_0 - C\left(1 + \frac{2}{e^{\frac{\hbar\omega_0}{2k_BT}} - 1}\right) \quad (2)$$

$$\Gamma_{\rm ph}(T) = \Gamma_0 + \Gamma\left(1 + \frac{2}{e^{\frac{\hbar\omega_0}{2k_BT}} - 1}\right), \quad (3)$$

where C and Γ are positive constants, ω_0 is the bare phonon frequency, and Γ_0 is a residual, temperature-independent linewidth. From the fits, we extract $\omega_0 = 137.1$ cm^{-1}, $C = 0.1755$ cm^{-1}, $\Gamma_0 = 3.496$ cm^{-1} and $\Gamma = 0.05918$ cm^{-1} for the A_g peak at 128.8 cm^{-1}. Similarly, the position and linewidth of the B_g peak at 61.6 cm^{-1} is well fitted with the formulae with $\omega_0 = 64.96$ cm^{-1}, $C = 0.153$ cm^{-1}, $\Gamma_0 = 1.614$ cm^{-1} and $\Gamma = 0.02442$ cm^{-1}.

Ignoring the A_g peak at 89.9 cm^{-1}, we could conclude the absence of CDW in this system. However, as shown in figure 3(a), the linewidth of the A_g peak at 89.9 cm^{-1} fitted with a single Lorentzian function exhibits an unusual increase, almost exponential, upon cooling. To emphasize this point, we show in the inset of figure 3(c) the spectra of this peak at 5 K obtained from two different samples and two different laser excitations. Interestingly, the peak splits into two peaks at low temperature, which can explain the unusual increase of the linewidth observed upon cooling. It is important to notice that the peak at 89.9 cm^{-1} has the A_g symmetry and is by definition non-degenerate. In addition, no other peak that we did not observe is expected around that energy. The observation of a new peak is thus most likely caused by a lowering of the symmetry of the system. In that sense, the new peak emerging at low temperature may be related to the CDW-like gap feature observed at 4 K by STM [5]. Indeed, the A_g phonon at 89.9 cm^{-1} represents the vibration of Te^1, Te^2, Te^5, Te^6, Te^7 and Te^8, among which are atoms located at the bright and dark stripes observed by Du *et al* in STM measurements [2], where the CDW-like gap feature is detected. If this is really the origin of the peak splitting, we estimate that the CDW transition temperature or the temperature at which CDW fluctuations emerge is somewhere between 140 K and 200 K, the temperature range where the linewidth of the 89.9 cm^{-1} starts to increase. Unfortunately, the proximity of the two-peak components prevents us from performing a reliable fit of the 89.9 cm^{-1} feature using two Lorentzian functions at such high temperature. Further experiments such as electron diffraction experiments should be done in the future to confirm the existence of the CDW and test its relationship to superconductivity.

4. Summary

In summary, we have performed polarized Raman scattering measurements on the newly discovered superconductor $Ta_4Pd_3Te_{16}$ ($T_c = 4.6$ K). We observe 28 out of 33 Raman active modes, with frequencies in good accordance with our first-principles calculations. Most of the phonons that we observe vary only slightly with temperature except for one A_g phonon at 89.9 cm^{-1}. The linewidth of the A_g phonon mode at 89.9 cm^{-1} shows an unconventional increase with temperature decreasing, which is possibly due to a CDW transition or to CDW fluctuations.

Acknowledgments

We acknowledge J Ma, P Zhang and J-X Yin for useful discussions. This work was supported by grants from MOST (2010CB923000, 2011CBA001000, 2011CBA00102, 2012CB821403 and 2013CB921703) and NSFC (11004232, 11034011/A0402, 11234014, 11274362 and 11474330) from China.

References

[1] Jiao W H, Tang Z T, Sun Y L, Liu Y, Tao Q, Feng C M, Zeng Y W, Xu Z A and Cao G H 2014 *J. Am. Chem. Soc.* **136** 1284–7

[2] Du Z, Fang D, Wang Z, Li Y, Du G, Yang H, Zhu X and Wen H-H 2015 *Sci. Rep.* **5** 9408

[3] Pan J, Jiao W H, Hong X C, Zhang Z, He L P, Cai P L, Zhang J, Cao G H and Li S Y 2015 *Phys. Rev.* B **92** 180505(R)
[4] Singh D J 2014 *Phys. Rev.* B **90** 144501
[5] Fan Q *et al* 2015 *Phys. Rev.* B **91** 104506
[6] Mar A and Ibers J A 1991 *J. Chem. Soc. Dalton Trans.* 639
[7] Alemany P, Jobic S, Brec R and Canadell E 1997 *Inorg. Chem.* **36** 5050–7
[8] Kroumova E, Aroyo M I, Perez-Mato J M, Kirov A, Capillas C, Ivantchev S and Wondratschek H 2003 *Phase Trans.* **76** 155–70
[9] Giannozzi P *et al* 2009 *J. Phys.: Condens. Matter* **21** 395502
[10] Perdew J P, Burke K and Ernzerhof M 1996 *Phys. Rev. Lett.* **77** 3865–8
[11] Baroni S, Giannozzi P and Testa A 1987 *Phys. Rev. Lett.* **58** 1861
[12] Baroni S, de Gironcoli S, Dal Corso A and Giannozzi P 2001 *Rev. Mod. Phys.* **73** 515
[13] Gonze X 1995 *Phys. Rev.* A **52** 1096
[14] Menéndez J and Cardona M 1984 *Phys. Rev.* B **29** 2051
[15] Klemens P G 1966 *Phys. Rev.* **148** 845–8